

Received July 30, 2020; reviewed; accepted September 28, 2020

## Microwave assistant synthesis of calcium phosphate minerals using hen's eggshells as a calcium source

Marta Kalbarczyk, Aleksandra Szcześ

Department of Interfacial Phenomena, Institute of Chemical Sciences, Faculty of Chemistry, Maria Curie-Skłodowska University in Lublin, Sq. M. Curie-Skłodowska 3, 20-031 Lublin, Poland

Corresponding author: [aszczes@poczta.umcs.lublin.pl](mailto:aszczes@poczta.umcs.lublin.pl) (A. Szcześ)

**Abstract:** In this study raw hen's eggshells were used as a calcium source for calcium phosphate mineral synthesis. The materials composed of brushite and different amounts of HA (hydroxyapatite) and  $\beta$ -TCP ( $\beta$ -tricalcium phosphate) with the needle-like, sheet-like and hexagonal structures were synthesized in the presence of the microwave. It was found that the time of microwave action, temperature and initial pH are parameters affecting the morphology and composition of the obtained materials, i.e. the increasing duration of MW exposure increases the amount of HA increases, whereas the temperature increase causes an increase in the contents of brushite and  $\beta$ -TCP. The lowering of initial pH leads to an increase in the brushite content.

**Keywords:** hydroxyapatite, brushite,  $\beta$ -TCP, microwave assisted synthesis

### 1. Introduction

Based on the development of many fields of medicine, among others orthopaedy and dentistry, the market is still open up for new biocompatible materials which could be used as a basic material of artificial bones and teeth. Finding out real reasons for different hard tissue diseases promotes preventive actions in everyday life to avoid undesirable effects (Fejerskov and Kidd, 2009).

The composition of human teeth and enamel was analysed due, among others, to receive crucial information about the interfacial behaviour with the microbial biofilm and its interactions with mouth hygiene products. The tooth enamel is a thin layer of highly mineralized tissue covering and protecting the surface of the teeth while the dentin is the inner part of tooth structure. The main component of both tissues are inorganic compounds including calcium phosphates, particularly carbonated calcium-deficient hydroxyapatite (Angervall et al., 1958). The enamel contains about 97% hydroxyapatite (HA) arranged in the highly orderly microstructure of thin, needle-like crystals bound via proteins whereas small amounts of such elements as sodium, calcium or magnesium were also detected (Gutiérrez-Salazar and Reyes-Gasga, 2003). In the term of health protection, pellicle, thin film of salivary proteins, carbohydrates and lipids which cover the enamel surface also play an essential role (Epple et al., 2019).

There are many components of commercial toothpastes known as protection against caries, dental defects or hypersensitivity, as well as improving the look of teeth. These are fluoride compounds like sodium monofluorophosphate, sodium fluoride or stannous fluoride (Clark-Perry and Levin, n.d.), bioactive glass (Wang et al., 2011), antiredeposition agents like polyphosphates or sodium citrate (Epple et al., 2019), surfactants like sodium lauryl sulfate (Epple et al., 2019), enzymes (e.g. bromelain) (Epple et al., 2019), peroxides (Fearon, 2007) or calcium phosphates such as hydroxyapatite (Gjorgievska et al., 2013; Nakahira et al., 1999; Tschoppe et al., 2011).

Finding new, quick and financially attractive procedures to obtain everyday health care products such as a toothpaste is still in the focus of scientists. The nano-sized hydroxyapatite crystals structure and morphology are compatible to the enamel ones. Moreover, small particles of nano-HA may be embedded in a structure of enamel filling small depressions and holes thereby promoting mouth health

protection (Pepla et al., 2014). It was also proved that nano-HA has a significant ability to link with proteins, components of biofilms and bacteria present on the tooth surface (Itthagarun et al., 2010).

According to the studies reported in the literature, the methods of obtaining hydroxyapatite can be divided into three main groups (Sadat-Shojai et al., 2013): dry methods including the solid-state reaction (Guo et al., 2013) and mechanochemical methods (Achar et al., 2017), wet methods like precipitation (Liu et al., 2001; Yelten-Yilmaz and Yilmaz, 2018), hydrolysis (Nakahira et al., 1999; Sinitsyna et al., 2005), sol-gel (Choi et al., 2020), hydrothermal (Chesley et al., 2020; Daryan et al., 2020) and employing high-temperature during synthesis, among others, procedures exploiting the combustion results (Batista et al., 2020) or pyrolysis (Sadat-Shojai et al., 2013) ( Fig. 1). It was highlighted that the synthesis method as well as the synthesis conditions have an essential influence on the composition and morphology of the product (Sadat-Shojai et al., 2013).

## CALCIUM PHOSPHATES SYNTHESIS METHODS

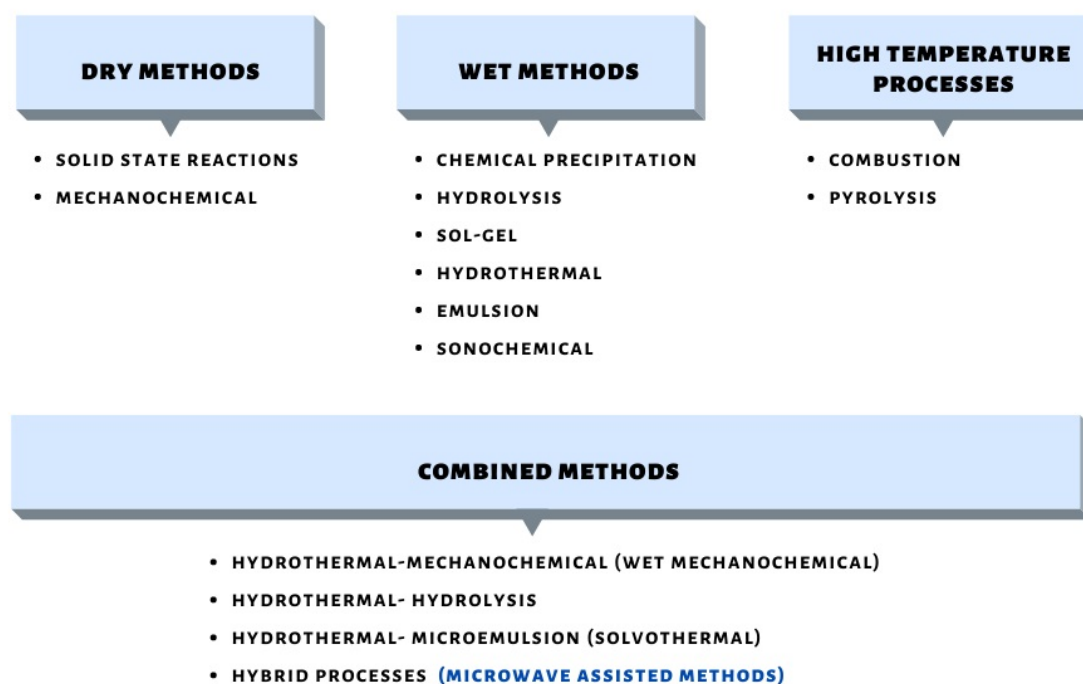


Fig. 1. Classification of calcium phosphates synthesis methods

Using the microwave (MW) assistance during the synthesis a pure hydroxyapatite phase as well as the biphasic calcium phosphate material were obtained (Hassan et al., 2016; Liang et al., 2013; Sikder et al., 2020). Kumar et al. (Kumar et al., 2012) obtained carbonated hydroxyapatite flower-like nanoparticles using hen's eggshells and microwave irradiation. A characteristic shape of nanoparticles was due to the introduction of EDTA (edetic acid) as a modifying agent. Shavandi et al. (Shavandi et al., 2015) published the results of nano-crystalline hydroxyapatite synthesis utilizing mussel shells and using microwaves in the synthesis procedure. They employed a high-temperature furnace during shells preparation and they obtained pure hydroxyapatite crystals with nano-rod morphology and faceted surfaces of about 15-20 nm width and diameter and 30-70 nm length as their final product. Derkus et al. (Derkus et al., 2016) presented a mixed synthesis method combining microwave irradiation with ultrasonification. The obtained nano-HA particles were classified as spherical with the average diameter of 60-80 nm. Apalangya et al. (Apalangya et al., 2018) described nano-hydroxyapatite synthesized by the fast microwave irradiation of partially etched eggshell particles using the ball-milling method with two sets of stainless-steel balls. Grinding eggshells gave a characteristic, oblong shape and the obtained nano-HA using as-prepared eggshells powder presented uniform needle-like morphology.

Owing to the green chemistry trends recommending reduction of synthetic chemicals usage, as well as energy input, the scientists started to study biogenic precursors of synthesis substrates. One of the

main streams is to replace a synthetic source of calcium by the natural, one originating from wastes as animal bones e.g. bovine (Niakan et al., 2015), pig (Ofudje et al., 2018) or chicken (Bee and Hamid, 2019), natural shells e.g. abalone (Huang et al., 2020), snails (Zhou et al., 2016), oyster (Almukarramah and Yusuf, 2020), mussels (Edralin et al., 2017), meti (Ruslan et al., 2020), clam (Bramhe et al., 2014) and eggshells (De Angelis et al., 2017; Malau and Adinugraha, 2020).

The aim of this study was to obtain calcium phosphate nanoparticles composed mainly of hydroxyapatite that could be employed as a profitable toothpaste component, by the hydrothermal method using microwaves irradiation during the synthesis. The natural source of the calcium was raw hen's eggshells without boiling or calcination prior to synthesis. It helped to reduce the energy input by eliminating the calcination and heating steps. The composition and morphology of the obtained materials were analysed in terms of duration and temperature of microwave irradiation as well as the initial pH of the calcium solution.

## 2. Materials and methods

### 2.1. Materials

HNO<sub>3</sub>, NaOH, Na<sub>2</sub>HPO<sub>4</sub> purchased from AVANTOR S.A. (Poland) were used in the studies. All the solutions was prepared with water purified by the use of Millipore Q-Plus 185 system. The hen's eggshells were collected from the household, washed in distilled water and dried overnight at 60°C. The clean and dry material was crushed in a mortar to obtain fine, homogeneous powder.

### 2.2. Synthesis

The synthesis without microwaves was prepared as follows: the washed, dried and grated eggshells (1.7585g) were dissolved in 15 ml of 1M nitric acid and stirred for 1 hour using a magnetic stirrer (500 rpm). The pH of the mixture was adjusted to 12 and then a 40 ml of 0.3M Na<sub>2</sub>HPO<sub>4</sub> solution was added using the peristaltic pump with the flow rate equal 20ml/min. The synthesis was conducted by stirring the solution for 4 hours under room conditions. The suspension was exposed at 60°C for 24 hours without mixing. The precipitate was then filtered, washed with ethanol and dried at 50°C.

To determine the influence of microwaves after the addition of Na<sub>2</sub>HPO<sub>4</sub> solution, the resulting solutions were subjected to microwave irradiation in the CEM 5 MARS microwave oven (Canada) working with magnetron frequency 2455MHz and power equal to 800W. Reaction mixtures were subjected to the microwave irradiation for 5, 10 and 15 minutes at the constant temperature of 60°C and 140°C in the oven during exposure. Just after the exposure to the microwaves the suspensions were filtered, washed with ethanol and dried at 60°C.

### 2.3. Material characterization

The composition of the obtained products was determined by Infrared Spectroscopy with Fourier Transformation - FTIR (Inqry Molecular Nicolet IS 10, Thermo Scientific, USA) and X- ray diffraction analysis (XRD) using the powder diffractometer Empyrean (PANalytical).

The morphology was studied by Scanning Electron Microscopy (Quanta 3D FEG, FEI).

The specific surface area was calculated using the BET approach from the adsorption of gaseous nitrogen at -196°C after out-gassing of the samples at 200°C (ASAP 2420 V 2.09 analyser, Micromeritics Inc, USA).

## 3. Results and discussion

### 3.1. The impact of microwave operating time

In the first step the effect of time of exposure to microwaves irradiation for 5, 10 and 15 minutes was studied. The IR and XRD spectra are shown in Fig. 2.

The main bands originating from the characteristic stretching vibrations of the PO<sub>4</sub><sup>3-</sup> groups ( $\nu_1$ - $\nu_4$ ) are observed for all product spectra (Fig. 2a). The analysis of the peaks shape on the spectra of the materials occurring at 1100-500cm<sup>-1</sup> indicates that the products are at least two-phase materials. In the case of the

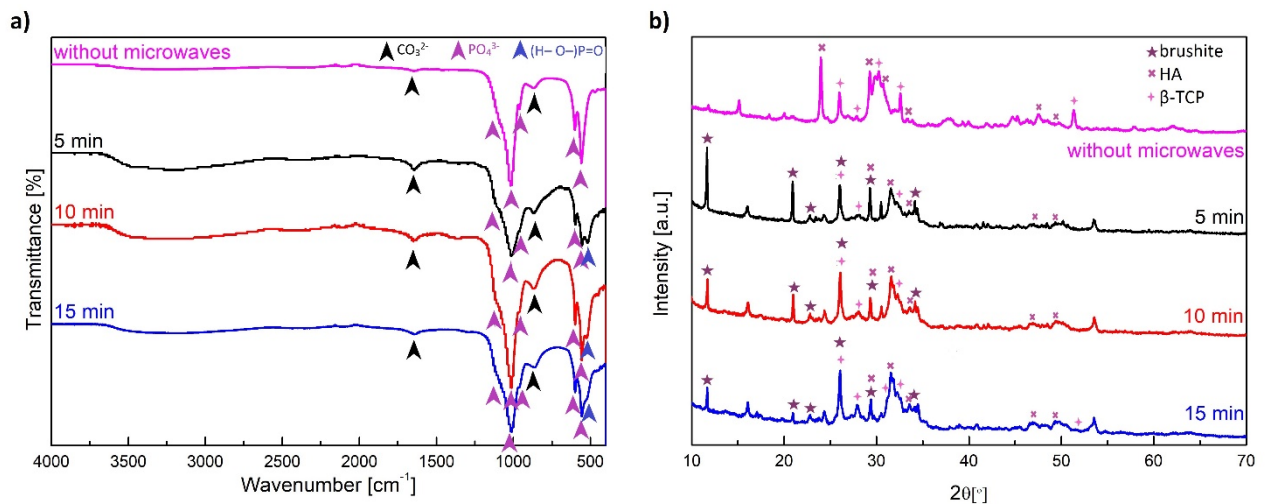


Fig. 2 FTIR spectra (a) of the obtained materials and their XRD patterns (b)

material obtained without the microwaves the presence of  $\beta$ -TCP bands in the range 1100-550  $\text{cm}^{-1}$  and the lack of peaks characteristic of pure HA derived from the hydroxyl bonds at positions 3570  $\text{cm}^{-1}$  and 630  $\text{cm}^{-1}$  prove that during the synthesis the dehydroxylation process took place and formed HA was partially transformed into  $\beta$ -TCP (Tanimoto et al., 2005).

It can be seen that the microwave irradiation time is a crucial factor in the synthesis of calcium phosphates. The material obtained from the 5 min exposure to microwaves exhibits characteristic peaks shapes and positions of peaks in the wavelength range 600-500 $\text{cm}^{-1}$  with the maximum at 603  $\text{cm}^{-1}$ , 559  $\text{cm}^{-1}$  originating from the bending vibrations of  $\text{PO}_4^{3-}$  hydroxyapatite groups (Rehman and Bonfield, 1997; Sajahan and Wan Ibrahim, 2014) as well as the bonding vibrations (H - O-) P = O at 517  $\text{cm}^{-1}$  (Binitha and Pradyumnan, 2013; Hirsch et al., 2014; Sánchez-Enríquez and Reyes-Gasga, 2013). This confirms the presence of acidic phosphate groups characteristic of brushite. The wide band at about 1014  $\text{cm}^{-1}$  characterized by a large intensity corresponds to the triple degenerate asymmetric P-O stretching vibrations, while the peak with the maximum at 960  $\text{cm}^{-1}$  corresponds to the non-degenerate symmetrical vibrations stretching P-O bonds. The peak observed at the wave number of 870  $\text{cm}^{-1}$ , corresponding to the bending vibrations of the C-O bonds comes from the  $\text{CO}_3^{2-}$  group, and that at 1640  $\text{cm}^{-1}$  comes from the carbonate group stretching vibrations (Rehman and Bonfield 1997; Sajahan and Wan Ibrahim 2014). The presence of carbonate groups signals confirms the substitution of phosphate ions by the carbonate ones in the crystals lattice. A wide peak in the 3500-3000  $\text{cm}^{-1}$  range associated with the OH- stretching vibrations is characteristic of the OH acidic groups present inside the crystals. With the extension of the microwave time the composition of the product changed. It can be noticed that there are differences in the wave number range of 600-400  $\text{cm}^{-1}$ . The shape of the peaks in the mentioned area as well as the presence of a signal of lower intensity at a wavelength of about 520  $\text{cm}^{-1}$  for the synthesis with 10 minutes of irradiation and its vanishing for the synthesis with a longer microwave exposure time suggest a decrease in the brushite content in the analyzed material. The hydroxyl stretching signal in the range of 3500-2500  $\text{cm}^{-1}$  is observed to decline. Moreover, the signal intensity at 1640  $\text{cm}^{-1}$  from the  $\text{CO}_3^{2-}$  groups decreases with the microwave time extension. All these changes can be associated with the transformation of the brushite phase into more temperature and mechanically resistant calcium phosphate, i.e.  $\beta$ -TCP.

The results of the FTIR spectra analysis were confirmed by the XRD studies (Fig. 2b) of obtained precipitates. In the product spectra characteristic peaks for hydroxyapatite are observed in the positions for each material at 26.0°, 31.6°, 32.0°, 34.0°, 46.2° and 49.3° (Ahmed and Ahsan 2008; Krithiga and Sastry 2011). There are differences between the microwaved and non-microwaved materials in the diffraction images. The intensity of peaks at 31.8° and 34.0° is higher for the non-microwaved product and results from the overlapped HA and  $\beta$ -TCP signals. The main peaks corresponding to the  $\beta$ -TCP structure occur in the positions of 26.7°, 31.1° and 34.5° (Tanimoto et al., 2005).

The spectrum of the material after 5 minutes of microwaves treatment presents also peaks characteristic of brushite, i.e.: 11.5°, 20.9°, 22.7°, 29.3°, 34.5° (Binitha and Pradyumnan, 2013; Lee and Kumta, 2010). It can be seen that the intensity of those signals decreases significantly with the increasing time of MW action indicating the gradual disappearance of brushite with the extension of the microwave action during the synthesis. Moreover, the differences in the ratio of intensity of peaks characteristic of HA and brushite are also visible. This can be associated with a decrease in the content of brushite phase relative to hydroxyapatite one with the increasing time of exposition to microwaves.

The SEM pictures of the materials are presented in Fig. 3. It can be noticed that the mineral synthesized without microwaves (Fig. 3a) consists mostly of fine rod-like crystals combined into larger, compact agglomerates interspersed with single flakes in the hexagonal shape. The needle-like crystals look like hydroxyapatite crystals (Apalangya et al., 2018; Ibrahim et al., 2015) while the hexagonal ones can be  $\beta$ -TCP. It is shown that after the 5 minute irradiation (Fig. 3b) irregular sheet-like components considered as brushite (LeGeros et al., 2003) phase predominate in the structure with fine, flower-like fragments all around the sheets. With the time extension of microwave treatment to 10 (Fig. 3c) and 15 (Fig. 3d) minutes the amount and size of sheet-like structures decreased and more rod-like elements appeared, which can confirm that the increase of hydroxyapatite content in the material increases with the extending time of microwave usage. The microwave treatment for 15 minutes was considered as the optimal time for further studies.

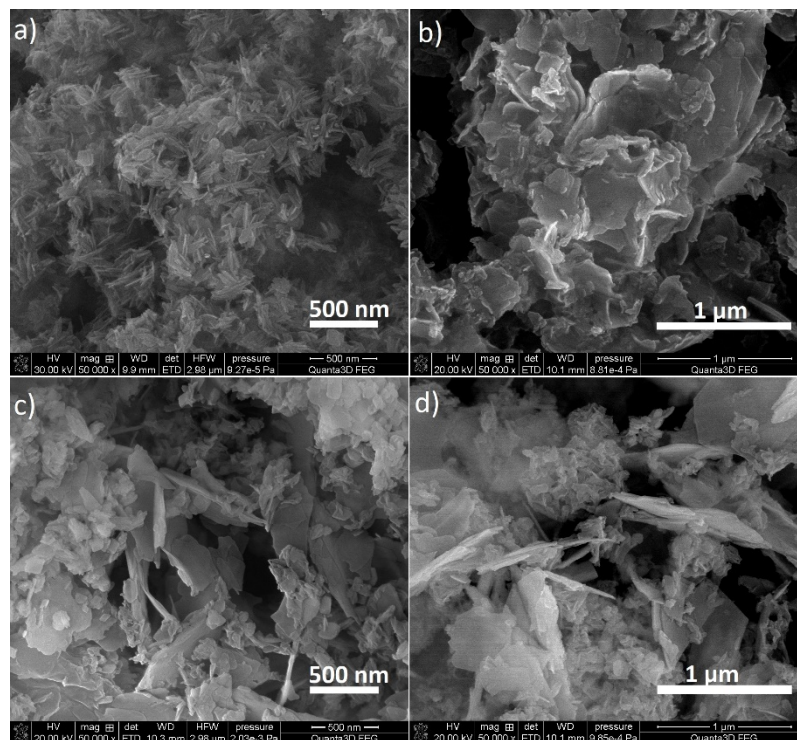


Fig. 3. SEM pictures of the material without (a) and with microwave treatment during the synthesis for: 5 (b) 10 (c) and 15 (d) minutes

### 3.2. The impact of temperature and pH

The effect of temperature increase during the microwave irradiation was also studied and the results are presented in Fig. 4. The composition of the precipitates obtained at 60°C and 140°C was investigated. It can be noticed that the temperature increase caused weakening of the signal from the carbonate groups in the range of 1500-1400  $\text{cm}^{-1}$  as well as at 870  $\text{cm}^{-1}$  and the lack of peak in the range of 3500-3000  $\text{cm}^{-1}$  (Fig. 4a). Moreover, the (H - O-) P = O band at 517  $\text{cm}^{-1}$  characteristic of the brushite phase is observed.

More details of the composition changes due to different temperatures are delivered from the XRD spectra analysis (Fig 4b). The higher intensity of peaks originating from the  $\beta$ -TCP at 11.5° as well as at 20.9° indicates that with the higher synthesis temperature the material contains a greater amount of

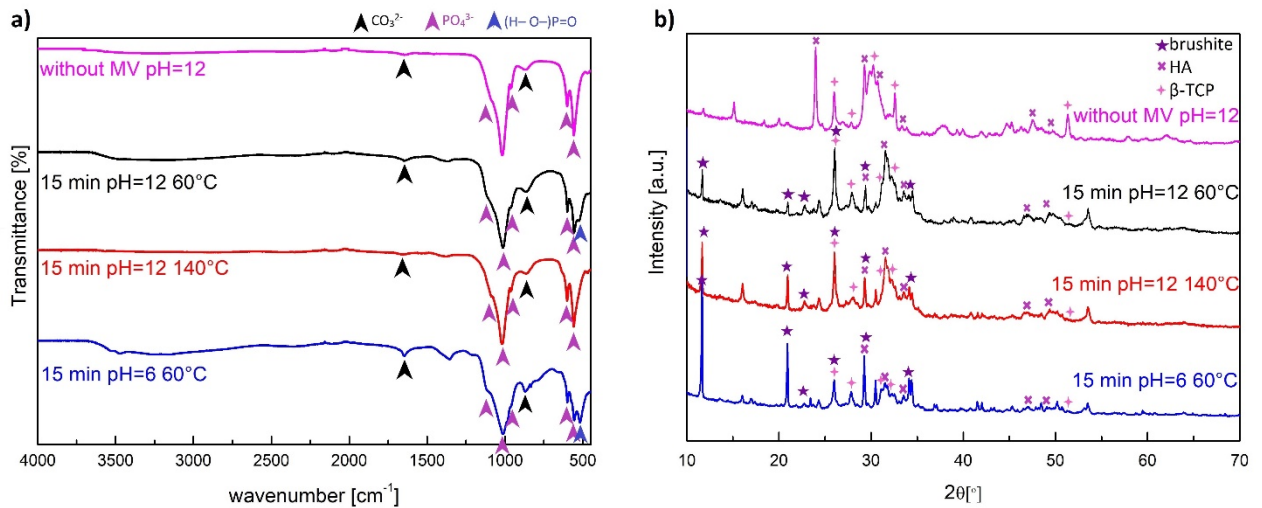


Fig. 4. FTIR spectra (a) and XRD patterns (b) of the materials obtained at different microwave irradiation temperatures and initial pH values of the solution

brushite. A higher intensity of signal at  $31.1^\circ$  originating from the  $\beta$ -TCP phase is also observed. This indicates that with the temperature increase during the microwave irradiation, the content of  $\beta$ -TCP in the material also increases, which can be caused by a higher temperature and mechanical resistance of  $\beta$ -TCP phase.

The SEM pictures (Fig. 5a, b, c, d) show that at the higher temperature of microwave irradiation the structure of the product contains more rod-like elements. Moreover, those structures seem to be larger than in the case of the material obtained without the microwave support. Therefore, the content of sheet-like crystals decreased significantly with the increasing microwaves temperature.

In order to study the effect of initial pH of the solution on the product composition the synthesis was also carried out with the initial pH equal 6. The FTIR spectra (Fig. 4a) indicate that the initial pH of the solution has a strong impact on the crystal form of the obtained calcium phosphate. The characteristic peak with the maximum at  $518\text{ cm}^{-1}$  as well as higher intensity for the signals from the hydroxyl groups suggest that the synthesis in the weakly acidic medium leads to an increase of brushite content in the

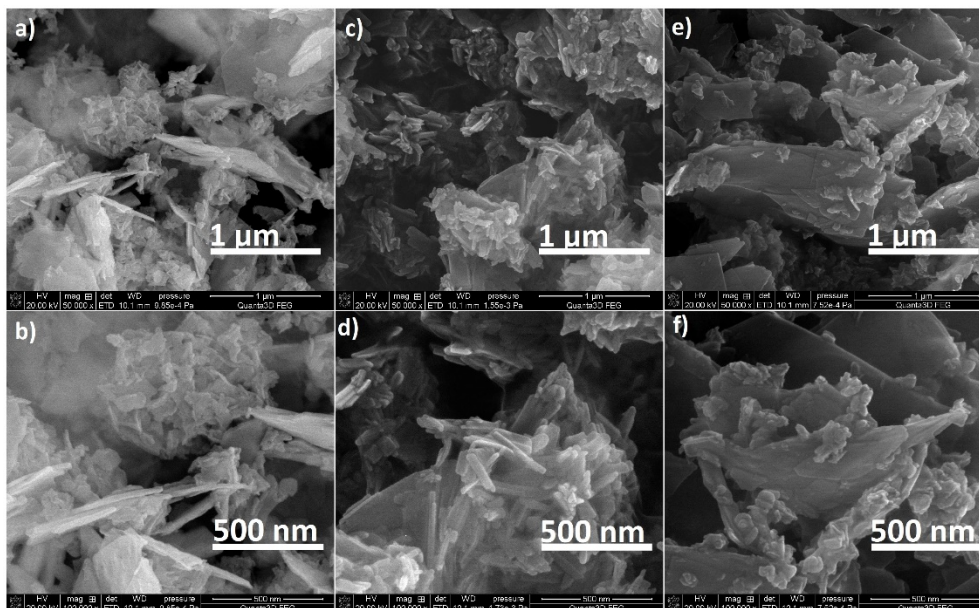


Fig. 5. SEM pictures of the materials treated with MW for 15 minutes: a,b) at  $60^\circ\text{C}$  initial pH=12, c,d) at  $140^\circ\text{C}$ , initial pH = 12 and e,f)  $60^\circ\text{C}$ , initial pH=6

material. Moreover, at lower pH value the higher contamination with carbonate groups in the crystal lattice can be observed as a stronger signal from the carbonate groups at  $1640\text{ cm}^{-1}$  and  $870\text{ cm}^{-1}$ . The XRD patterns (Fig. 4b) of those materials confirmed the conclusions from the FTIR spectra analysis. The signals at  $11.5$ ,  $20.9$ ,  $29.2$  and  $34.1^\circ$  originating from the brushite phase increase significantly with the initial pH decrease. Moreover, characteristic peak positions for  $\beta$ -TCP and HA are observed. There is also a confirmation in the SEM picture (Fig. 5e,f) where it is shown that in the weakly acidic medium there are more flat sheet-like structures typical of brushite. Moreover, the rod-like parts are shorter and exhibit a more irregular and amorphous form in comparison with the SEM pictures of the product obtained in the synthesis with the alkaline medium at the beginning of the process (Fig. 5a,b).

The pore size and distribution as well as the surface area of the adsorbents are considered one of the most important parameters describing adsorbents quality because they provoke the ability to retain particles. Structural parameters of the materials synthesized at initial pH=12 without and with microwave irradiation for 15 min. at  $60^\circ\text{C}$  were determined using the nitrogen adsorption and desorption isotherms. From the obtained data the BET specific surface area, the total pore volume, the average pore diameter and volume were determined using the BET as well as Barret, Joyner, Halenda (BJH) methods. The obtained results are summarized in Table 1 while the graphs of  $\text{N}_2$  adsorption/desorption isotherms are presented in Fig. 6.

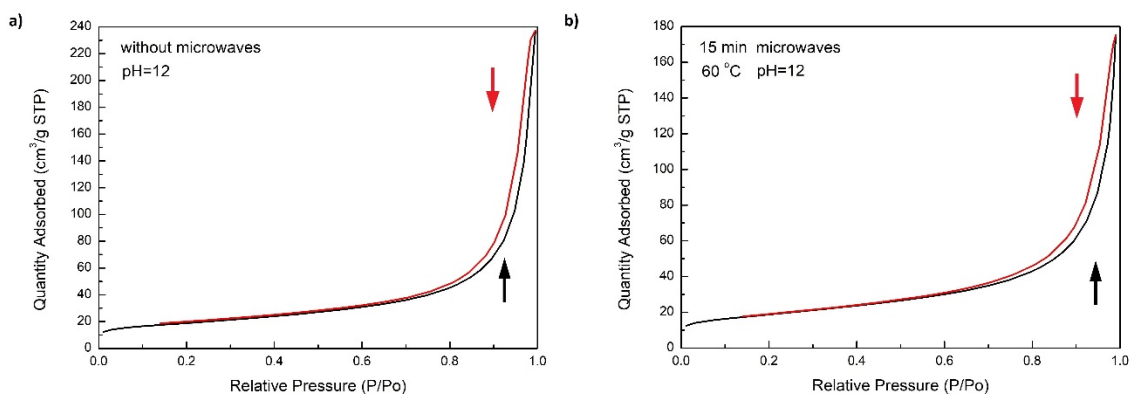


Fig. 6.  $\text{N}_2$  adsorption/ desorption isotherms of the materials obtained: a) without MW and b) with MF action

According to the IUPAC classification the obtained isotherms are type IV, characteristic of mesoporous materials on which the process of physisorption occurs. This isotherm type is associated with the multilayer adsorption followed by the capillary condensation, characterized by the H3 hysteresis loop and the tendency to reach the limit of adsorption values in the area of high pressure  $p/p_0$ , as well as monolayer/multilayer adsorption attributes at the beginning of the curve. A clear jump at  $p/p_0=0.90-0.98$  indicates a wide pore size distribution. Structural parameters of the obtained materials are similar while they are slightly lower for the product of microwave-assisted synthesis.

Table 1. Structural parameters of the obtained materials

	Without MW	With MW
Specific surface area BET [ $\text{m}^2/\text{g}$ ]	66.1	65.6
Total pore volume [ $\text{cm}^3/\text{g}$ ]	0.37	0.27
Micropores volume [ $\text{cm}^3/\text{g}$ ]	0.0061	0.0055
Average pore size BET [nm]	22.2	16.5
Pores diameter from the adsorption BJH [nm]	25.3	19.3
Pores diameter from the desorption BJH [nm]	24.1	18.5

The specific surface area and the total pore volume are large for both products. Similar values of these parameters were obtained using both synthetic calcium source precursors and related natural resources, however, with higher energy inputs and more complicated synthesis processes (Akram et al., 2015; Chen et al., 2020; Yudin et al., 2019). The contribution of micropores in the entire pore volume is

small hence it can be concluded that the materials exhibit a mesoporous nature of the structure what is desired for those used as industry adsorbents. Large values of the surface area and the total pore volumes are the results of crystals morphology. Minerals obtained without MW are composed of agglomerates formed from rod-like crystals with a size less than 200 nm and single hexagonal flakes (Fig. 3a). While the sample obtained with MW radiation consist mainly of sheet-like structures of larger size (around 500nm) and rod-like crystals (Fig. 3d). Moreover, the number of aggregates is smaller. This is reflected in a slightly smaller specific surface area but significantly smaller total pore volume and pore diameter.

The material obtained in this study using microwave assisted synthesis of calcium phosphate using eggshells as a calcium biosource consists of three different crystal forms: hydroxyapatite, brushite and  $\beta$ -TCP. Comparing with literature data, the materials obtained as the results of similar synthesis procedures consist mostly of one or two phases, mainly hydroxyapatite with mostly homogenous morphology and characteristic for different synthesis conditions nanocrystals shapes (Apalangya et al., 2018; Hassan et al., 2016; Kumar et al., 2012; LeGeros et al., 2003; Liang et al., 2013; Shavandi et al., 2015; Sikder et al., 2020). In our study the mixture of rod-like, hexagonal and flake-like structures was obtained. Biphasic materials are mostly the mixture of hydroxyapatite and  $\beta$ -TCP (Hassan et al., 2015; Park et al., 2008; Sampath Kumar et al., 2000). Brushite exhibits high stability at acidic pH (3.5-6.5) and was proved to be osteoconductive and hard tissue biocompatible (Jayasree et al., 2019). Its metastable character can be desirable in the terms of to be calcium and phosphate ions deliverer during enamel rebuilding.

The main reason for obtaining different results may be the use of shells without thermal (calcination) or chemical treatment in our study. Most of the cited literature studies have been carried out using calcined eggshells. High temperature removes organic impurities present in raw shells. Based on the thermogravimetric study (results not shown here), it was found that the used eggshells contain about 5% of organic impurities that decompose in the temperature range from 200 to 650°C. Therefore, in future research, the synthesis will be carried out on shells without organic impurities.

#### 4. Conclusions

In the study calcium phosphate materials were obtained using prevalent gastronomical wastes such as hen's eggshells which is desirable from economical and environmental points of view. The FTIR and XRD studies indicated that material obtained without MW is composed of HA and  $\beta$ -TCP. The MW assisted synthesis led to the three-component material of needle-like, sheet-like and hexagonal structures containing mainly brushite and different amounts of HA and  $\beta$ -TCP. Using the microwave irradiation leads to creation of larger, flake-like structures. With the increasing duration of MW exposure, the amount of HA increases. The temperature increase during the operation of MW causes an increase in the contents of brushite and  $\beta$ -TCP. The initial pH lowering to 6 causes an increase in the brushite content. The 15 min. action of MW gives a material with the similar specific surface area but with the pores of smaller total pore volume and average size.

It can be seen that not only the time of MW action but also the initial pH and temperature are crucial factors affecting the final materials composition and structure. Structural parameters of the obtained minerals (nano size, high specific surface are and its needle like shape) suggest their potential application as a beneficial toothpaste component.

The next step of research will be to use other natural sources of calcium originating from wastes, as snails, as well as natural surfactants for the synthesis of HA with controlled size and shape.

#### Acknowledgement

We would like to thank Professor Renata Łyszczek for providing MW equipment.

#### References

- ACHAR, T.K., BOSE, A., MAL, P., 2017. *Mechanochemical synthesis of small organic molecules*. Beilstein J. Org. Chem. 13, 1907-1931.
- AKRAM, M., ALSHEMARY, A.Z., GOH, Y.-F., WAN IBRAHIM, W.A., LINTANG, H.O., HUSSAIN, R., 2015.

- Continuous microwave flow synthesis of mesoporous hydroxyapatite*. Materials Science and Engineering: C 56, 356–362. <https://doi.org/10.1016/j.msec.2015.06.040>
- ALMUKARRAMAH, A., YUSUF, Y., 2020. *Development Carbonated Hydroxyapatite Powders from Oyster Shells (Crassostrea gigas) by Carbonate Content Variations [WWW Document]*. Materials Science Forum. <https://doi.org/10.4028/www.scientific.net/MSF.975.76>
- ANGERVALL, L., BERGER, S., ROCKERT, H., 1958. *A Microradiographic and X-Ray Crystallographic Study of Calcium in the Pineal Body and in Intracranial Tumours*. Acta Pathologica Microbiologica Scandinavica 44, 113–119.
- APALANGYA, V., RANGARI, V., JEELANI, S., DANKYI, E., YAYA, A., DARKO, S., 2018. *Rapid microwave synthesis of needle-like hydroxyapatite nanoparticles via template directing ball-milled spindle-shaped eggshell particles*. Ceramics International 44, 7165–7171.
- BATISTA, H.A., SILVA, F.N., LISBOA, H.M., COSTA, A.C.F.M., 2020. *Modeling and optimization of combustion synthesis for hydroxyapatite production*. Ceramics International 46, 11638–11646.
- BEE, S.-L., HAMID, Z.A.A., 2019. *Characterization of chicken bone waste-derived hydroxyapatite and its functionality on chitosan membrane for guided bone regeneration*. Composites Part B: Engineering 163, 562–573.
- BINITHA, M.P., PRADYUMNAN, P.P., 2013. *Dielectric Property Studies of Biologically Compatible Brushite Single Crystals Used as Bone Graft Substitute*. J. Biomat. Nanobiotechnol. 04(02), 119–122.
- BRAMHE, S., KIM, T.N., BALAKRISHNAN, A., CHU, M.C., 2014. *Conversion from biowaste Venerupis clam shells to hydroxyapatite nanowires*. Materials Letters 135, 195–198.
- CHEN, J., LIU, J., DENG, H., YAO, S., WANG, Y., 2020. *Regulatory synthesis and characterization of hydroxyapatite nanocrystals by a microwave-assisted hydrothermal method*. Ceramics International 46, 2185–2193.
- CHESLEY, M., KENNARD, R., ROOZBAHANI, S., KIM, S.M., KUKK, K., MASON, M., 2020. *One-step hydrothermal synthesis with in situ milling of biologically relevant hydroxyapatite*. Materials Science and Engineering: C 113, 110962.
- CHOI, G., CHOI, A.H., EVANS, L.A., AKYOL, S., BEN-NISSAN, B., 2020. *A review: Recent advances in sol-gel-derived hydroxyapatite nanocoatings for clinical applications*. Journal of the American Ceramic Society, <https://doi.org/10.1111/jace.17118>
- CLARK-PERRY, D., LEVIN, L., 2020. *Comparison of new formulas of stannous fluoride toothpastes with other commercially available fluoridated toothpastes: A systematic review and meta-analysis of randomised controlled trials*. International Dental Journal n/a. <https://doi.org/10.1111/idj.12588>
- DARYAN, S.H., KHAVANDI, A., JAVADPOUR, J., 2020. *Surface engineered hollow hydroxyapatite microspheres: Hydrothermal synthesis and growth mechanisms*. Solid State Sciences 106, 106301.
- DE ANGELIS, G., MEDEGHINI, L., CPNTE, A.M., MIGNARDI, S., 2017. *Recycling of eggshell waste into low-cost adsorbent for Ni removal from wastewater*. Journal of Cleaner Production 164, 1497–1506.
- DERKUS, B., ARSLAN, Y.E., EMREGUL, K.C., EMREGUL, E., 2016. *Enhancement of aptamer immobilization using egg shell-derived nano-sized spherical hydroxyapatite for thrombin detection in neuroclinic*. Talanta 158, 100–109.
- EDRALIN, E.J.M., GARCIA, J.L., DELA ROSA, F.M., PUNZALAN, E.R., 2017. *Sonochemical synthesis, characterization and photocatalytic properties of hydroxyapatite nano-rods derived from mussel shells*. Materials Letters 196, 33–36.
- EPPLE, M., MEYER, F., ENAX, J., 2019. *A Critical Review of Modern Concepts for Teeth Whitening*. Dentistry Journal 7, 79.
- FEARON, J., 2007. *Tooth whitening: concepts and controversies*. J. Ir. Dent. Assoc. 53, 132–140.
- FEJERSKOV, O., KIDD, E., 2009. *Dental Caries: The Disease and Its Clinical Management*. John Wiley & Sons.
- GJORGIEVSKA, E.S., NICHOLSON, J.W., SLIPPER, I.J., STEVANOVIC, M.M., 2013. *Remineralization of Demineralized Enamel by Toothpastes: A Scanning Electron Microscopy, Energy Dispersive X-Ray Analysis, and Three-Dimensional Stereo-Micrographic Study*. Microscopy and Microanalysis 19, 587–595.
- GUO, X., YAN, H., ZHAO, S., LI, Z., LI, Y., LIANG, X., 2013. *Effect of calcining temperature on particle size of hydroxyapatite synthesized by solid-state reaction at room temperature*. Advanced Powder Technology 24, 1034–1038.
- GUTIERREZ-SALAZAR, M. del P., REYES-GASGA, J., 2003. *Microhardness and chemical composition of human tooth*. Materials Research 6, 367–373.
- HASSAN, M.N., MAHMOUD, M.M., EL-FATTAH, A.A., KANDIL, S., 2016. *Microwave-assisted preparation of Nano-hydroxyapatite for bone substitutes*. Ceramics International 42, 3725–3744.
- HASSAN, M.N., MAHMOUD, M.M., EL-FATTAH, A.A., KANDIL, S., 2015. *Microwave rapid conversion of sol-gel-derived hydroxyapatite into  $\beta$ -tricalcium phosphate*. J Sol-Gel Sci Technol 76, 74–81.
- HIRSCH, A., AZURI, I., ADDADI, L., WEINER, S., YANG, K., CURTAROLO, S., KRONIK, L., 2014. *Infrared*

- Absorption Spectrum of Brushite from First Principles*. Chem. Mater. 26, 2934–2942.
- HUANG, H., DU, M., CHEN, J., ZHONG, S., WANG, J., 2020. *Preparation and characterization of abalone shells derived biological mesoporous hydroxyapatite microspheres for drug delivery*. Materials Science and Engineering: C 113, 113–120.
- IBRAHIM, A.-R., ZHOU, Y., LI, X., CHEN, L., HONG, Y., SU, Y., WANG, H., LI, J., 2015. *Synthesis of rod-like hydroxyapatite with high surface area and pore volume from eggshells for effective adsorption of aqueous Pb(II)*. Materials Research Bulletin 62, 132–141.
- ITTHAGARUN, A., KING, N., CHEUNG, Y.M., 2010. *The effect of nano-hydroxyapatite toothpaste on artificial enamel carious lesion progression: An in-vitro pH-cycling study*. Hong Kong Dental Journal 7, 61–66.
- JAYASREE, R., KUMAR, T.S.S., VENKATESWARI, R., NANKAR, R.P., DOBLE, M., 2019. *Eggshell derived brushite bone cement with minimal inflammatory response and higher osteoconductive potential*. J Mater Sci: Mater Med 30, 113–120.
- KUMAR, G.S., THAMIZHAVEL, A., GIRIJA, E.K., 2012. *Microwave conversion of eggshells into flower-like hydroxyapatite nanostructure for biomedical applications*. Materials Letters 76, 198–200.
- LEE, D., KUMTA, P.N., 2010. *Chemical synthesis and stabilization of magnesium substituted brushite*. Materials Science and Engineering: C 30, 934–943.
- LEGEROS, R.Z., LIN, S., ROHANIZADEH, R., MIJARES, D., LEGEROS, J.P., 2003. *Biphasic calcium phosphate bioceramics: preparation, properties and applications*. Journal of Materials Science: Materials in Medicine 14, 201–209.
- LIANG, T., QIAN, J., YUAN, Y., LIU, C., 2013. *Synthesis of mesoporous hydroxyapatite nanoparticles using a template-free sonochemistry-assisted microwave method*. J. Mater. Sci. 48, 5334–5341.
- LIU, C., HUANG, Y., SHEN, W., CUI, J., 2001. *Kinetics of hydroxyapatite precipitation at pH 10 to 11*. Biomaterials 22, 301–306.
- MALAU, N.D., ADINUGRAHA, F., 2020. *Synthesis of hydrokxyapatite based duck egg shells using precipitation method*. J. Phys.: Conf. Ser. 1563, 012020.
- NAKAHIRA, A., SAKAMOTO, K., YAMAGUCHI, S., KANENO, M., TAKEDA, S., OKAZAKI, M., 1999. *Novel Synthesis Method of Hydroxyapatite Whiskers by Hydrolysis of alpha-Tricalcium Phosphate in Mixtures of Water and Organic Solvent*. Journal of the American Ceramic Society 82, 2029–2032.
- NIAKAN, A., RAMESH, S., GANESAN, P., TAN, C.Y., PURBOLAKSONO, J., CHANDRAN, H., RAMESH, S., TENG, W.D., 2015. *Sintering behaviour of natural porous hydroxyapatite derived from bovine bone*. Ceramics International 41, 3024–3029.
- OFUDJE, E.A., RAJENDRAN, A., ADEOGUN, A.I., IDOWU, M.A., KAREEM, S.O., PATTANAYAK, D.K., 2018. *Synthesis of organic derived hydroxyapatite scaffold from pig bone waste for tissue engineering applications*. Advanced Powder Technology 29, 1–8.
- PARK, Y.M., RYU, S.C., YOON, S.Y., STEVENS, R., PARK, H.C., 2008. *Preparation of whisker-shaped hydroxyapatite/ $\beta$ -tricalcium phosphate composite*. Materials Chemistry and Physics 109, 440–447.
- PEPLA, E., BESHARAT, L.K., PALAIA, G., TENORE, G., MIGLIAU, G., 2014. *Nano-hydroxyapatite and its applications in preventive, restorative and regenerative dentistry: a review of literature*. Ann Stomatol (Roma) 5, 108–114.
- REHMAN, I., BONFIELD, W., 1997. *Characterization of hydroxyapatite and carbonated apatite by photo acoustic FTIR spectroscopy*. Journal of Materials Science: Materials in Medicine 8, 1–4. <https://doi.org/10.1023/A:1018570213546>
- RUSLAN, HARDI, J., KHAIRUDDIN, DEFLINDA, RISKAWATI, 2020. *Synthesis of hydroxyapatite from meti shells (batissa violecea l. Von Lamarck 1818) by wet precipitation method*. J. Phys.: Conf. Ser. 1434, 012023.
- SODAT-SHOJAI, M., KHORASANI, M.-T., DINPANAHI-KHOSHDARGI, E., JAMSHIDI, A., 2013. *Synthesis methods for nanosized hydroxyapatite with diverse structures*. Acta Biomaterialia 9, 7591–7621.
- SAJAHAN, N.A., WAN IBRAHIM, W.M.A., 2014. *Microwave Irradiation of Nanohydroxyapatite from Chicken Eggshells and Duck Eggshells [WWW Document]*. The Scientific World Journal. <https://doi.org/10.1155/2014/275984>
- SAMPATH KUMAR, T.S., MANJUBALA, I., GUNASEKARAN, J., 2000. *Synthesis of carbonated calcium phosphate ceramics using microwave irradiation*. Biomaterials 21, 1623–1629.
- SANCHEZ-ENRIQUEZ, J., REYES-GASGA, J., 2013. *Obtaining  $\text{Ca}(\text{H}_2\text{PO}_4)_2 \cdot \text{H}_2\text{O}$ , monocalcium phosphate monohydrate, via monetite from brushite by using sonication*. Ultrasonics Sonochemistry 20, 948–954.
- SHAVANDI, A., BEKHIT, A.E.-D.A., ALI, A., SUN, Z., 2015. *Synthesis of nano-hydroxyapatite (nHA) from waste mussel shells using a rapid microwave method*. Materials Chemistry and Physics 149–150, 607–616.
- SIKDER, P., REN, Y., BHADURI, S.B., 2020. *Microwave processing of calcium phosphate and magnesium phosphate based orthopedic bioceramics: A state-of-the-art review*. Acta Biomaterialia 111, 29–53.

- SINITSYNA, O.V., VERESOV, A.G., KOVALEVA, E.S., KOLEN'KO, Y.V., PUTLYAEV, V.I., TRETYAKOV, Y.D., 2005. *Synthesis of hydroxyapatite by hydrolysis of  $\alpha$ -Ca<sub>3</sub>(PO<sub>4</sub>)<sub>2</sub>*. Russian Chemical Bulletin 1, 79–86.
- TANIMOTO, Y., HAYAKAWA, T., NEMOTO, K., 2005. *Tape-casting technique can prepare  $\beta$ -TCP sheets with uniform thickness and flexibility*. Journal of Biomedical Materials Research Part B: Applied Biomaterials 73B, 157–163.
- TSCHOPPE, P., ZANDIM, D.L., MARTUS, P., KIELBASSA, A.M., 2011. *Enamel and dentine remineralization by nano-hydroxyapatite toothpastes*. Journal of Dentistry 39, 430–437.
- WANG, Z., JIANG, T., SAURO, S., PASHLEY, D.H., TOLEDANO, M., OSORI, R., LIANG, S., XING, W., SA, Y., WANG, Y., 2011. *The dentine remineralization activity of a desensitizing bioactive glass-containing toothpaste: an in vitro study*. Australian Dental Journal 56, 372–381.
- YELTEN-YILMAZ, A., YILMAZ, S., 2018. *Wet chemical precipitation synthesis of hydroxyapatite (HA) powders*. Ceramics International 44, 9703–9710.
- YUDIN, A., ILINYKH, I., CHUPRUNOV, K., KOLESNIKOV, E., KUZNETSOV, D., LEYBO, D., GODYMCHUK, A., 2019. *Microwave treatment and pH influence on hydroxyapatite morphology and structure*. J. Phys.: Conf. Ser. 1145, 012003.
- ZHOU, H., YANG, M., ZHANG, M., HOU, S., KONG, S., YANG, L., DENG, L., 2016. *Preparation of Chinese mystery snail shells derived hydroxyapatite with different morphology using condensed phosphate sources*. Ceramics International 42, 16671–16676.